Solving 2D multi-crack problems with arbitrary distribution by virtual boundary meshless least squares method

***Qiang Xu[1]**

[1]Department of Building Engineering, Tongji University, Shanghai 200092, China.

*Corresponding author: xuqiang@tongji.edu.cn

Abstract

This paper is about how solving two dimensional multi-crack problems with arbitrary distribution by the virtual boundary meshless least squares method. In this article, the local domain where a single crack is contained would be treated as twain subdomain when solving multi-crack problem. And this method incorporates the point interpolation method (PIM) with the compactly supported radial basis function (CSRBF) often used in boundary-type meshless methods to approximately construct the virtual source function on the virtual boundary corresponding to each subdomain. According to the definition about sub-domain in this paper, the added extra sub-domains on the boundary extended along the crack surface as "conventional sub-domain method" in the direct boundary element method do not have to be considered, thereby reducing the computational, especially avoiding this calculation error caused due to inadequate number of the elements or with the collocation points configured on the boundary of the additional sub-domains and its improper configuration. In addition, since the configuration of virtual boundary has a certain preparability, the integration along the virtual boundary can be carried out over the smooth simple curve that can be structured beforehand (for 2D problems) to reduce the complicity and difficulty of calculus without loss of accuracy, while ''Vertex Question'' existing in BEM can be avoided.

Keywords: Virtual boundary, Meshless, Least squares, Radial basis function, Multi-crack

1. Introduction

Generally speaking, crack, multi-crack or micro-crack are pre-existed in engineering components [1] and structures [2], brittle or quasi-brittle materials, and so on. As is known to all, the stress intensity factor can be used to describe the stress field of the crack tip and predict crack growth in fracture mechanics. So the stress intensity factor for the calculation of a crack or multi-crack analysis also is very important. In fact, the equation with solving crack problem is easily established, but the exact solution is quite difficultly obtained, especially in multi-crack problems. That is, the analytic methods, such as the westergaard method [3], the complex variable function method [4], conformal mapping [5] and so on, can only solve the simple or regular crack problem, and complex or irregular crack problems need resort to numerical methods.

The boundary element method (BEM) is an important kind of numerical methods, and it is suitable for analyzing a large field gradient function of the problem and also can better calculate the stress concentration. Some scholars solve the crack problems by the BEM, such as Z.H. Yao, P.B. Wang and H.T. Wang et al. [6-7] use dual BEM to analyze the numerous micro-cracks, Q.H. Qin and Y.W. Mai [8] employ the BEM for crack-hole problems in thermopiezoelectric materials, E.D. Leonel and W.S. Venturini [9] use the dual boundary element formulation to analysis of multi-fractured domains, X.Q. Yan [10] analyzes the stress intensity factors of multiple circular arc cracks in a plane elasticity plate by employing the BEM, and so on. But the BEM still has its own drawbacks. It is shown that the coefficient matrix is asymmetric and its construction is time consuming in the process of calculation. In addition, the treatment of singular integration is inconvenient and takes much more time, and there is mimicry singular integral whilst reducing calculating precision, especially when solving the related physics quantities on the boundary, which

is called “Boundary Layer Effect”. Fortunately, the virtual boundary element least square method proposed by the authors in the literature [11-19] can avoid above described drawbacks in BEM, since its coefficient matrix is symmetric and it does not involve singular integral.

According to the definition about sub-domain in this paper, the added extra sub-domains on the boundary extended along the crack surface as “conventional sub-domain method” in the direct boundary element method do not have to be considered, thereby reducing the computational, especially avoiding this calculation error caused due to inadequate number of the elements or with the collocation points configured on the boundary of the additional sub-domains and its improper configuration. In addition, since the configuration of virtual boundary has a certain preparability, the integration along the virtual boundary can be carried out over the smooth simple curve that can be structured beforehand (for 2D problems) to reduce the complicity and difficulty of calculus without loss of accuracy, while ‘‘Vertex Question’’ existing in BEM can be avoided.

The rest of the paper is organized as follows. In Section 2, the radial point interpolation method and the stress intensity factor are described in brief. In Section 3, the calculation scheme for solving multi-crack problems by virtual boundary meshless least squares method is derived in detail, and the related processing technologies in the calculation of multi-crack problems are introduced. In Section 4, numerical examples are presented to demonstrate the efficiency and validity of the method proposed in the paper. Finally, a summary is given in Section 5 to conclude this paper.

2. The radial point interpolation method and the stress intensity factor

2.1 The radial point interpolation method

Consider a scalar function $u(\boldsymbol{x})$ defined in the problem domain Ω, the approximation function $u^h(\boldsymbol{x})$ of u(x) is represented by a set of scattered interpolation nodes, and $u^h(\boldsymbol{x})$ can approximates $u(\boldsymbol{x})$ at a point of interest $\boldsymbol{x}$. By the reference [16], the RPIM function interpolation expression augmented with polynomials can be rewritten as [20-27]

$$u^h(\boldsymbol{x}) = \sum_{i=1}^{n} R_i(\boldsymbol{x}) a_i + \sum_{j=1}^{m} p_j(\boldsymbol{x}) b_j = \mathbf{R}^{\mathrm{T}}(\boldsymbol{x})\mathbf{a} + \mathbf{p}^{\mathrm{T}}(\boldsymbol{x})\mathbf{b} \tag{1}$$

In which, $R_i(\boldsymbol{x})$ is the compactly supported radial basis function (CSRBF) proposed by Wu [28], n is the number of RBFs in the defined domain of the calculation point $\boldsymbol{x}$, namely

$$R_i(\boldsymbol{x}) = \tilde{r}^4(4 + 16r + 12r^2 + 3r^3) \tag{2}$$

where $r = \|\boldsymbol{x} - \boldsymbol{x}_i\|/d_i$, in which d_i is the dimension of the local support domain for CSRBF (shown in Fig. 1), and

$$\tilde{r} = \begin{cases} (1-r) & \text{for } 0 \le r \le 1 \\ 0 & \text{other} \end{cases} \tag{3}$$

and $p_j(\boldsymbol{x})$ is polynomial basis functions in two-dimensional coordinates $\boldsymbol{x}^{\mathrm{T}} = [x, y]$, m is the number of polynomial basis functions. The vector $\mathbf{a}$ of coefficients for RBFs is $\{a_1 \quad a_2 \quad \cdots \quad a_n\}^{\mathrm{T}}$, and the vector $\mathbf{b}$ of coefficients for polynomial is $\{b_1 \quad b_2 \quad \cdots \quad b_m\}^{\mathrm{T}}$. Then, coefficients a_i and b_j are constants yet to be determined.

In order to determine a_i and b_j in Eq. (1), a support domain is formed for the point of interest at $\boldsymbol{x}$, and n field nodes are included in the support domain. Coefficients a_i and b_j in Eq. (1) can be determined by enforcing Eq. (1) to be satisfied at these n nodes surrounding the point of interest $\boldsymbol{x}$. Then, the $n+m$ unknown coefficients a_i and b_j in Eq. (1) can be obtained by the following equations

$$\sum_{i=1}^{n} R_i(\boldsymbol{x}_I)a_i + \sum_{j=1}^{m} p_j(\boldsymbol{x}_I)b_j = u_s(\boldsymbol{x}_I) \qquad I = 1,2,\cdots,n \tag{4}$$

$$\sum_{I=1}^{n} p_j(\boldsymbol{x}_I)a_I = 0 \qquad j = 1,2,\cdots,m \tag{5}$$

where Eq. (5) is m constraint conditions added using the orthogonality between $p_j(\boldsymbol{x}_I)$ ($I = 1,2,\cdots,n$) and $\mathbf{a}$ to solve $n+m$ variables in Eq. (1). Combing Eqs. (4) and (5) yields the following set of equations in the matrix form

$$\mathbf{B}\begin{Bmatrix}\mathbf{a}\\ \mathbf{b}\end{Bmatrix} = \begin{Bmatrix}\mathbf{u}_s\\ \mathbf{0}\end{Bmatrix} \tag{6}$$

where the moment matrix $\mathbf{B}$ is

$$\mathbf{B} = \begin{bmatrix} R_1(\boldsymbol{x}_1) & \cdots & R_n(\boldsymbol{x}_1) & p_1(\boldsymbol{x}_1) & \cdots & p_m(\boldsymbol{x}_1) \\ \vdots & \ddots & \vdots & \vdots & \ddots & \vdots \\ R_1(\boldsymbol{x}_n) & \cdots & R_n(\boldsymbol{x}_n) & p_1(\boldsymbol{x}_n) & \cdots & p_m(\boldsymbol{x}_n) \\ p_1(\boldsymbol{x}_1) & \cdots & p_1(\boldsymbol{x}_n) & 0 & \cdots & 0 \\ \vdots & \ddots & \vdots & \vdots & \ddots & \vdots \\ p_m(\boldsymbol{x}_1) & \cdots & p_m(\boldsymbol{x}_n) & 0 & \cdots & 0 \end{bmatrix} \tag{7}$$

Using Eq. (6) and by Eq. (1), we can obtain

$$u^h(\boldsymbol{x}) = \begin{Bmatrix}\mathbf{R}^{\mathrm{T}}(\boldsymbol{x}) & \mathbf{p}^{\mathrm{T}}(\boldsymbol{x})\end{Bmatrix}\mathbf{B}^{-1}\begin{Bmatrix}\mathbf{u}_s\\ \mathbf{0}\end{Bmatrix} = \tilde{\mathbf{N}}^{\mathrm{T}}(\boldsymbol{x})\begin{Bmatrix}\mathbf{u}_s\\ \mathbf{0}\end{Bmatrix} \tag{8}$$

where the vector $\mathbf{u}_s$ of function values is $\begin{Bmatrix}u_1 & u_2 & \cdots & u_n\end{Bmatrix}^{\mathrm{T}}$, and the RPIM shape functions can be expressed as

$$\begin{aligned}\tilde{\mathbf{N}}^{\mathrm{T}}(\boldsymbol{x}) &= \begin{Bmatrix}\mathbf{R}^{\mathrm{T}}(\boldsymbol{x}) & \mathbf{p}^{\mathrm{T}}(\boldsymbol{x})\end{Bmatrix}\mathbf{B}^{-1} \\ &= \begin{Bmatrix}N_1(\boldsymbol{x}) & N_2(\boldsymbol{x}) & \cdots & N_n(\boldsymbol{x}) & N_{n+1}(\boldsymbol{x}) & \cdots & N_{n+m}(\boldsymbol{x})\end{Bmatrix}\end{aligned} \tag{9}$$

And the RPIM shape functions $\mathbf{N}(\boldsymbol{x})$ corresponding to the nodal displacements vector $\mathbf{u}_s$ are obtained as

$$\mathbf{N}^{\mathrm{T}}(\boldsymbol{x}) = \begin{Bmatrix}N_1(\boldsymbol{x}) & N_2(\boldsymbol{x}) & \cdots & N_n(\boldsymbol{x})\end{Bmatrix} \tag{10}$$

Therefore, Eq. (8) can be rewritten as

$$u^h(\boldsymbol{x}) = \mathbf{N}^{\mathrm{T}}(\boldsymbol{x})\mathbf{u}_s = \sum_{i=1}^{n} N_i u_i \tag{11}$$

In this paper, in order to further improve the accuracy and computational efficiency, the idea of RPIM with CSRBF is incorporated to approximately construct the virtual source function $\varphi_k(\boldsymbol{\xi})$ ($k = 1,2$) in VBEM.

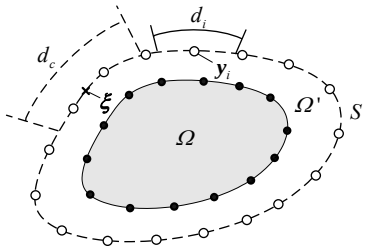

Figure 1. Computing model of single domain problem for the meshless VBEM

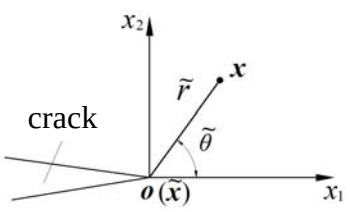

Figure 2. Local coordinate description of the crack tip displacement

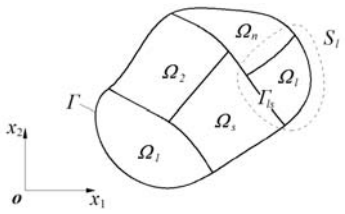

Figure 3. Diagrammatic sketch of multi-

2.2 The stress intensity factor

In a given 2D Cartesian coordinate system, for the composite crack problems with containing Ⅰ and Ⅱ type, the displacement u_1 and u_2 along x_1、 x_2 direction at crack tip point $\tilde{\boldsymbol{x}}$ can be expressed respectively as (shown in Fig. 2)

$$u_1 = \frac{K_{\mathrm{I}}}{2G}\sqrt{\frac{\tilde{r}}{2\pi}}\cos\frac{\tilde{\theta}}{2}\left(\kappa - 1 + 2\sin^2\frac{\tilde{\theta}}{2}\right) + \frac{K_{\mathrm{II}}}{2G}\sqrt{\frac{\tilde{r}}{2\pi}}\sin\frac{\tilde{\theta}}{2}\left(\kappa + 1 + 2\cos^2\frac{\tilde{\theta}}{2}\right) \tag{12}$$

$$u_2 = \frac{K_{\mathrm{I}}}{2G}\sqrt{\frac{\tilde{r}}{2\pi}}\sin\frac{\tilde{\theta}}{2}\left(\kappa + 1 - 2\cos^2\frac{\tilde{\theta}}{2}\right) + \frac{K_{\mathrm{II}}}{2G}\sqrt{\frac{\tilde{r}}{2\pi}}\cos\frac{\tilde{\theta}}{2}\left(-\kappa + 1 + 2\sin^2\frac{\tilde{\theta}}{2}\right) \tag{13}$$

In which, K_{I} and K_{II} are the stress intensity factors respectively corresponding to Ⅰ and Ⅱ type; $\tilde{r}$ is the distance between the calculation point $\boldsymbol{x}$ and the crack tip point $\tilde{\boldsymbol{x}}$, $\tilde{\theta}$ is the angle between the radial vector $\tilde{r}$ and the axis x_1; in addition, $G = E/2(1+\nu)$, and $\kappa = 3-4\nu$ (Plane strain problem), $\kappa = (3-\nu)/(1+\nu)$ (Plane stress problem).

By Eqs. (12) and (13), when $\tilde{\theta}$ turn counterclockwise an angle π, the displacement along x_1、 x_2 direction at the crack tip point $\tilde{\boldsymbol{x}}$ can be denoted respectively as

$$u_{1+} = \frac{K_{\mathrm{II}}}{2G}\sqrt{\frac{\tilde{r}}{2\pi}}(\kappa+1),\quad u_{2+} = \frac{K_{\mathrm{I}}}{2G}\sqrt{\frac{\tilde{r}}{2\pi}}(\kappa+1) \tag{14}$$

and, when $\tilde{\theta}$ turn clockwise an angle π, the corresponding displacement is

$$u_{1-} = -\frac{K_{\mathrm{II}}}{2G}\sqrt{\frac{\tilde{r}}{2\pi}}(\kappa+1),\quad u_{2-} = -\frac{K_{\mathrm{I}}}{2G}\sqrt{\frac{\tilde{r}}{2\pi}}(\kappa+1) \tag{15}$$

By Eqs. (14) and (15) simultaneous solution, K_{I} and K_{II} can be obtained, namely

$$K_{\mathrm{I}} = \frac{(u_{2+}-u_{2-})G}{\kappa+1}\sqrt{\frac{2\pi}{\tilde{r}}},\quad K_{\mathrm{II}} = \frac{(u_{1+}-u_{1-})G}{\kappa+1}\sqrt{\frac{2\pi}{\tilde{r}}} \tag{16}$$

For ease of comparison to the stress intensity factor K by different loads and under different geometric scales, need to introduce dimensionless stress intensity factor F. From the reference [29], $F = K/(\sigma\sqrt{\pi a})$, in which σ is a reference stress and a is crack half-length.

3. The calculation scheme for solving multi-crack problems

The idea for solving the multi-domain problems (shown in Fig. 3) by virtual boundary meshless least squares method has been given in the reference [16], and the virtual source function on the virtual boundary about each subdomain is approximately constructed by the boundary-type radial point interpolation method [20]. Here, according to basic idea of the literature [16], the idea for solving multi-crack problems is presented. According to the literature [16], there is

$$\boldsymbol{J}[\varphi^{(1)}(\boldsymbol{\xi}),\varphi^{(2)}(\boldsymbol{\xi}),\cdots,\varphi^{(n)}(\boldsymbol{\xi})] =$$

$$\sum_{l=1}^{n}\sum_{i=1}^{2}\left\{\sum_{j=1}^{N_u^l}\alpha_l\left[u_i^{(l)}(\boldsymbol{x}_j)-\overline{u}_i^{(l)}(\boldsymbol{x}_j)\right]^2\Bigg|_{\boldsymbol{x}_j\in\Gamma_l^u\cap\Gamma} + \sum_{j=N_u^l+1}^{N_u^l+N_P^l}\beta_l\left[p_i^{(l)}(\boldsymbol{x}_j)-\overline{p}_i^{(l)}(\boldsymbol{x}_j)\right]^2\Bigg|_{\boldsymbol{x}_j\in\Gamma_l^p\cap\Gamma}\right\} +$$

$$\sum_{G(\Gamma_{ks})}\sum_{i=1}^{2}\left\{\sum_{j=1}^{M_G}\alpha_J\left[u_i^{(k)}(\boldsymbol{x}_j)-u_i^{(s)}(\boldsymbol{x}_j)\right]^2\Bigg|_{\boldsymbol{x}_j\in\Gamma_{ks}^G} + \sum_{j=1}^{M_G}\beta_J\left[p_i^{(k)}(\boldsymbol{x}_j)+p_i^{(s)}(\boldsymbol{x}_j)\right]^2\Bigg|_{\boldsymbol{x}_j\in\Gamma_{ks}^G}\right\} \tag{17}$$

In which, $\boldsymbol{J}[\varphi^{(1)}(\boldsymbol{\xi}),\varphi^{(2)}(\boldsymbol{\xi}),\cdots,\varphi^{(n)}(\boldsymbol{\xi})]$ is the square deviation functional of the multi-domain composite problem about virtual source function $\varphi_k^{(i)}(\boldsymbol{\xi})$ ($k=1,2$; $i=1,2,\cdots,n$), and the above equation established must satisfies the given actual boundary conditions of the original problem and the corresponding connection conditions between the adjacent subdomains at the same time. n is

the number of subdomains within the problem given. $\Gamma_l^u \bigcap \Gamma$ and $\Gamma_l^p \bigcap \Gamma$ are called the exterior displacement and traction boundary of Ω_l, respectively, N_u^l is the number of real boundary nodes whose displacement is known on the boundary $\Gamma_l \bigcap \Gamma$ (namely $\Gamma_l^u \bigcap \Gamma$), while N_p^l the nodes number of known traction with outward normal direction on the boundary $\Gamma_l^p \bigcap \Gamma$; $\overline{u}_i^{(l)}(\boldsymbol{x}_j)$ and $\overline{p}_i^{(l)}(\boldsymbol{x}_j)$ are the known displacement and traction values along i^{th} direction at the j^{th} boundary point $\boldsymbol{x}_j$ on the exterior boundary $\Gamma_l^u \bigcap \Gamma$ and $\Gamma_l^p \bigcap \Gamma$ of l^{th} subdomain, respectively; α_l and β_l are weight coefficient about the displacement and traction of the l^{th} subdomain, respectively; G is the overall serial number of the current internal boundary Γ_{ks} (namely Γ_{ks}^G), M_G is the over-fulfilled collocation number on Γ_{ks}^G, α_J and β_J are weight coefficient about the displacement and traction on Γ_{ks}^G, respectively. By solving Eq. (17), the virtual source function $\varphi_k^{(l)}(\boldsymbol{\xi})$ ($k=1,2$; $l=1,2,\cdots,n$) can be obtained. As soon as the virtual source function $\varphi_k^{(l)}(\boldsymbol{\xi})$ is known, the corresponding physical value at $\boldsymbol{x}$ about each subdomain can be calculated through the following equations, namely

$$u_i^{(l)}(\boldsymbol{x}) = \int_{S_l} u_{ik}^*(\boldsymbol{x},\boldsymbol{\xi})\varphi_k^{(l)}(\boldsymbol{\xi})dS \tag{18}$$

$$\varepsilon_{ij}^{(l)}(\boldsymbol{x}) = \int_{S_l} \varepsilon_{ijk}^*(\boldsymbol{x},\boldsymbol{\xi})\varphi_k^{(l)}(\boldsymbol{\xi})dS \tag{19}$$

$$\sigma_{ij}^{(l)}(\boldsymbol{x}) = \int_{S_l} \sigma_{ijk}^*(\boldsymbol{x},\boldsymbol{\xi})\varphi_k^{(l)}(\boldsymbol{\xi})dS \tag{20}$$

$$p_i^{(l)}(\boldsymbol{x}) = \int_{S_l} \sigma_{ijk}^*(\boldsymbol{x},\boldsymbol{\xi})n_j\varphi_k^{(l)}(\boldsymbol{\xi})dS \tag{21}$$

It can be known from Eqs. (18) and (21), Eq. (17) is the square deviation functional about virtual source function $\varphi_k^{(i)}(\boldsymbol{\xi})$ ($k=1,2$; $i=1,2,\cdots,n$) that is the unknown function on the virtual boundary S_i. Unlike the conventional VBEM, 'virtual boundary meshless' mentioned in the paper means that the virtual source approximate functions $\tilde{\varphi}_k^{(i)}(\boldsymbol{\xi})$ ($k=1,2$; $i=1,2,\cdots,n$) constructed in the meshless VBEM are not dependent upon the geometric mesh generation of the computing element. That is to say, the idea of RPIM with CSRBF is incorporated to approximately construct the virtual source function. And a kind of background-mesh can be employed about the numerical integration of virtual source function in the method. Such as Eqs. (18) and (21), the virtual boundary S_l will be separated into m_e elements and there are e_g Gauss spots within each element, then their Gauss numerical integral of $u_i^{(l)}(\boldsymbol{x})$ and $p_i^{(l)}(\boldsymbol{x})$ can be expressed respectively as

$$\begin{aligned} u_i^{(l)}(\boldsymbol{x}) \approx \int_{S_l} u_{ik}^*(\boldsymbol{x},\boldsymbol{\xi})\tilde{\varphi}_k^{(l)}(\boldsymbol{\xi})dS &= \sum_{e=1}^{m_e^l}\sum_{g=1}^{e_e^l} \tilde{w}(\boldsymbol{\xi}_g^e)u_{ik}^*(\boldsymbol{x},\boldsymbol{\xi}_g^e)\tilde{\varphi}_k^{(l)}(\boldsymbol{\xi}_g^e) \\ &= \sum_{e=1}^{m_e^l}\sum_{g=1}^{e_e^l} \tilde{w}(\boldsymbol{\xi}_g^e)u_{ik}^*(\boldsymbol{x},\boldsymbol{\xi}_g^e)\mathbf{N}^{(l)\mathrm{T}}(\boldsymbol{\xi}_g^e)\cdot {}_s\tilde{\boldsymbol{\varphi}}_k^{(l)} \end{aligned} \tag{22}$$

$$\begin{aligned} p_i^{(l)}(\boldsymbol{x}) \approx \int_{S_l} \sigma_{ijk}^*(\boldsymbol{x},\boldsymbol{\xi})n_j\tilde{\varphi}_k^{(l)}(\boldsymbol{\xi})dS &= \sum_{e=1}^{m_e}\sum_{g=1}^{e_g} \tilde{w}(\boldsymbol{\xi}_g^e)\sigma_{ijk}^*(\boldsymbol{x},\boldsymbol{\xi}_g^e)n_j\tilde{\varphi}_k^{(l)}(\boldsymbol{\xi}_g^e) \\ &= \sum_{e=1}^{m_e}\sum_{g=1}^{e_g} \tilde{w}(\boldsymbol{\xi}_g^e)\sigma_{ijk}^*(\boldsymbol{x},\boldsymbol{\xi}_g^e)n_j\mathbf{N}^{(l)\mathrm{T}}(\boldsymbol{\xi}_g^e)\cdot {}_s\tilde{\boldsymbol{\varphi}}_k^{(l)} \end{aligned} \tag{23}$$

Substitute Eq. (22) and Eq. (23) into Eq. (17), then we can see that $\boldsymbol{J}[\varphi^{(1)}(\boldsymbol{\xi}),\cdots,\varphi^{(n)}(\boldsymbol{\xi})]$ will change as the vector of the entire virtual source function values ${}_s\tilde{\boldsymbol{\varphi}}^{(l)}$ ($l=1,2,\cdots,n$), so $\boldsymbol{J}[\varphi^{(1)}(\boldsymbol{\xi}),\cdots,\varphi^{(n)}(\boldsymbol{\xi})]$ can be expressed as $\boldsymbol{J}[{}_s\tilde{\boldsymbol{\varphi}}^{(1)}, {}_s\tilde{\boldsymbol{\varphi}}^{(2)},\cdots, {}_s\tilde{\boldsymbol{\varphi}}^{(n)}]$. In order to obtain the solution ${}_s\tilde{\boldsymbol{\varphi}}^{(l)}$ ($l=1,2,\cdots,n$), the variation is being made for Eq. (25), namely

$$\delta \boldsymbol{J} = 0 \tag{24}$$

Let *Ns* be node number on all virtual boundaries of multi-domain complex issues, then the

unknown vector of entire node function values $\boldsymbol{A}$ can be recorded as a unified manner, namely

$$\boldsymbol{A}=\left\{ {}_{s}\tilde{\boldsymbol{\varphi}}^{(1)\mathrm{T}},{}_{s}\tilde{\boldsymbol{\varphi}}^{(2)\mathrm{T}},\cdots,{}_{s}\tilde{\boldsymbol{\varphi}}^{(n)\mathrm{T}}\right\}^{\mathrm{T}}=\left\{ {}_{1}\tilde{\varphi}_{1}\quad {}_{1}\tilde{\varphi}_{2}\quad {}_{2}\tilde{\varphi}_{1}\quad {}_{2}\tilde{\varphi}_{2}\quad\cdots\quad {}_{Ns}\tilde{\varphi}_{1}\quad {}_{Ns}\tilde{\varphi}_{2}\right\}^{\mathrm{T}}$$
$$=\left\{\tilde{\varphi}_{1}\quad\tilde{\varphi}_{2}\quad\cdots\quad\tilde{\varphi}_{2Ns}\right\}^{\mathrm{T}} \tag{25}$$

From Equation (24), we get the governing equation for solving the unknown virtual source function values at all nodes on all virtual boundaries. Equation (24) can be rewritten in matrix form as follows [16]

$$\boldsymbol{KA}=\boldsymbol{B} \tag{26}$$

In the above equation, $\boldsymbol{K}=\left[k_{st}\right]_{2Ns\times 2Ns}$ is a symmetric coefficient matrix; $\boldsymbol{A}$ is the vector of the unknown virtual source function values $(2Ns\times 1)$; $\boldsymbol{B}$ is the right term that can be obtained based on the boundary conditions.

Definition of crack subdomain

Suppose that is the number m of cracks contained in whole domain Ω, and the local domain of each crack is treated as two sub-domains. So whole domain is artificially divided into $2m+1$ sub-domains, in which the boundary Γ_{+}^{i} and Γ_{-}^{i} of each crack is respectively referred to as the upper and lower boundaries of the crack (or left and right boundaries), as shown in Figure 4. Respective sub-domain can be artificially defined corresponding to the boundary Γ_{+}^{i} or Γ_{-}^{i} of each crack, namely sub-domain Ω_{+}^{i} corresponding to Γ_{+}^{i}. That is, there is twain sub-domain corresponding to each crack. And sub-domain Ω^{*} is considered as "Substrate domain" in addition to the crack sub-domains defined.

On numerical implementation of this method terms, the definition of the configuration shape of the crack has a certain degree of arbitrariness, such as rectangular or semi-circular or semi-elliptical and so on. And the selection of its shape and size hardly affects the result of the calculation. Compared with "conventional sub-domain method" in the direct boundary element method [30], the added extra sub-domains on the boundary extended along the crack surface do not have to be considered according to the definition about sub-domain in the paper, thereby reducing the computational, especially avoiding this calculation error caused due to inadequate number of the elements or with the collocation points configured on the boundary of the additional sub-domains and its improper configuration.

Element division near the crack tip by equal proportions

Due to stress gradient with larger changes on the vicinity of the crack tip, therefore, how the elements are reasonably distributed on the actual boundary near the crack tip to get a better numerical solution will be very important. Through numerical integration practice, we decorate the desired nodes in order to define the elements required near the crack tip for the numerical integration based on "proportional" mathematical ideas in the paper, thereby decide the division and distribution of element near the crack tip. The ideas of the specific implementation: suppose that a is crack half-length, and denote $a=\overline{BA}$. Here, point A is regarded as the crack tip, the desired nodes a_i are arranged from point B to point A according to the calculation formula $a_i=(1-q^{i})a/(1-q^{n})$ $(i=1,2,\cdots,n;\ q\neq 1)$, in which q is scale factor. When $i=n$, the position corresponding to a_n is the crack tip A.

4. Numerical Examples

4.1 There is a through-wall crack with crack half-length $a=1$ mm at the center position of the plate of side length $l=100$ mm, as shown in Figure 5. The load of perpendicular to upper and lower plate

edge is uniform distribution of tension, and it is expressed as $\sigma = 1$ MPa . Young's modulus of elasticity E=2.1×10^6 MPa, Poisson's ratio v=0.3.

Now, employ the method proposed in this article to calculate the above issues. The problem can be artificially divided into three sub-domains, namely one referred to as the subdomain Ω^* of "Substrate domain" and the other two sub-domains Ω_+^1 and Ω_-^1 belonging to crack definition, as shown in Figure 6. For crack sub-domain Ω_+^1, 22 elements are divided on the crack boundary Γ_+^1 based on "proportional" mathematical ideas, and three internal boundaries corresponding to Ω_+^1 take straight line edge and its each one is divided into 20 elements. Then there are a total of 104 elements on all actual boundaries corresponding to Ω_+^1. However, for the virtual boundary S_+^1 of Ω_+^1, employ a circle configuration of radius $r_1 = 1.22$ mm, and 45 elements are evenly distributed on S_+^1. However, for sub-domain Ω_-^1, its actual and virtual boundaries are divided by using the same method as the processing subdomain Ω_+^1. For the subdomain Ω^* of "Substrate domain", its outer boundary Γ_S is formed by the four straight line edges and 20 elements on each one are evenly distributed, then the element implementation of its internal boundary, namely element number and distribution, should be the same as the division corresponding to crack subdomain. However, for Ω^*, exist simultaneously inner virtual boundary S_{in}^* and external one S_{ex}^*, and their configuration all are a circle with the radius $r_3 = 72$ mm and $r_4 = 1.9$ mm, respectively. And 45 elements are evenly distributed on S_{in}^* or S_{ex}^*. All nodes on inner and external virtual boundaries add up to 180, namely DOF number is 360.

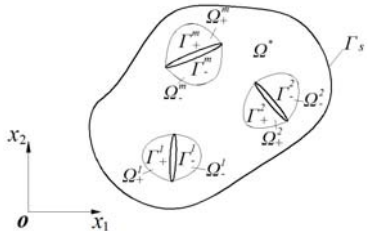

Figure 4. Diagrammatic sketch of containing multiple cracks

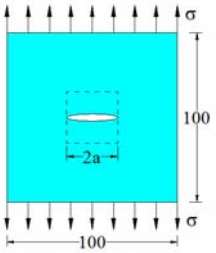

Figure 5. Calculation diagram of single crack

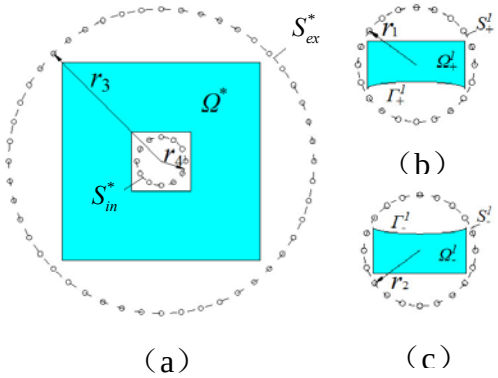

Figure 6. Discretization of single crack

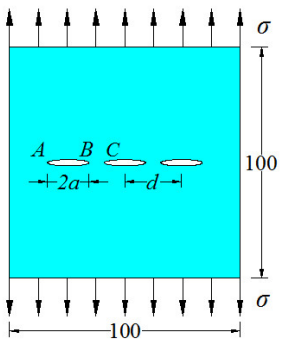

Figure 7. Calculation figure of three collinear cracks

With employing Westergaard' stress function method [29] to calculate the stress intensity factor of this example, the analytical solutions obtained is $\sqrt{\pi}$ MPa (=1.7725 MPa), and the numerical result in accordance with the method proposed in the paper for solving the stress intensity factor is 1.7758 MPa , its numerical error is 1.86‰. However, under the same degree of freedom, the comparison of the numerical results of the literature [31] about BEM J integral method and

displacement discontinuity method with the analytical solutions and the numerical solutions in the paper is shown in Table 1.

4.2 There are three collinear through-wall cracks with crack half-length $a=1$ mm of each crack for the plate with side length $l=100$ mm, as shown in Figure 7. The load of perpendicular to upper and lower plate edge is uniform distribution of tension, and it is expressed as $\sigma=1$ MPa. Young's modulus of elasticity E=2.1×10^6 MPa, Poisson's ratio v=0.3. In addition, the center distance of adjacent cracks denotes d, and the distance between adjacent crack tips is $2a/d$.

Now, employ the method proposed in this article to calculate the above issues. The problem can be artificially divided into seven sub-domains, namely one referred to as the subdomain Ω^* of "Substrate domain" and the other six sub-domains Ω_+^i and Ω_-^i (i=1,2,3) belonging to crack definition. Then the whole region Ω is divided into seven sub-domains, namely Ω_i ($i=1,2,\cdots,7$), and the discrete processing program on actual and virtual boundary of each subdomain is same as one of the previous example. However, the comparison of the numerical results of calculating the normalized stress intensity factor K_A, K_B, K_C at crack tip A, B, C. by the method proposed in the paper with them of employing the BEM with 45 displacement discontinuity element[32] and based on the stress function method[33] is shown in Table 2. And by comparison with the literature [32], the method proposed has fewer degrees of freedom for calculating the same problem, thus calculation efficiency can be improved. And the results of the method proposed is numerically more to be close to them of the literature [33] by comparison with the literature [32].

Tab.1 the stress intensity factor for the single crack

K	Analytical solution	J integral method [31]	Displacement discontinuity method [31]	The method of this paper
result (MPa)	1.7725	1.7867	1.9303	1.7758
error	——	8 ‰	8.9 %	1.86 ‰

Tab.2 the normalized stress intensity factor for three collinear cracks

F / $2a/d$	K_A			K_B			K_C		
	The paper	[32]	[33]	The paper	[32]	[33]	The paper	[32]	[33]
0.05	0.99885	0.9961	1.00083	0.99851	0.9961	1.00040	0.99876	0.9963	1.00063
0.1	0.99951	0.9972	1.00150	0.99959	0.9973	1.00164	1.00058	0.9982	1.00252
0.2	1.00370	1.0015	1.00585	1.00483	1.0026	1.00702	1.00799	1.0059	1.01030
0.3	1.01067	1.0085	1.01296	1.01480	1.0126	1.01710	1.02170	1.0195	1.02407
0.4	1.02058	1.0184	1.02297	1.03115	1.0288	1.03353	1.04285	1.0405	1.04529
0.5	1.03381	1.0317	1.03631	1.05666	1.0540	1.05913	1.07405	1.0714	1.07663
0.6	1.05118	1.0490	1.05383	1.09643	1.0932	1.09915	1.12046	1.1171	1.12316
0.7	1.07447	1.0722	1.07724	1.16144	1.1571	1.16456	1.19261	1.1881	1.19558
0.8	1.10743	1.1049	1.11032	1.27891	1.2724	1.28348	1.31668	1.3104	1.32136
0.9	1.16105	1.1581	1.16439	1.55727	1.5405	1.56454	1.59952	1.5835	1.60685

5. Conclusions

1. The ideas of the virtual boundary meshless least squares method with radial point interpolation have been formulated for solving multi-crack problems. However, the given numerical examples indicate its high accuracy and high efficiency.
2. The point interpolation scheme with compactly supported radial basis function is introduced into the method so that no element mesh is required in this method. Consequently, this method has the advantages of boundary-type meshless methods. It can be used for the calculation and analysis of complex question.
3. By comparison of “conventional sub-domain method” in the direct boundary element method, the added extra sub-domains on the boundary extended along the crack surface do not have to be considered according to the definition about sub-domain in the paper, thereby reducing the computational, especially avoiding this calculation error caused due to inadequate number of the elements or with the collocation points configured on the boundary of the additional sub-domains and its improper configuration.

References

[1] Z.H. Shi, M. Ohtsu, M. Suzuki, Y. Hibino, Numerical analysis of multiple cracks in concrete using the discrete approach, J. Struct. Eng-Asce, 127(9) (2001) 1085-1091.

[2] H. Qing, W. Yang, J. A. Lu, Numerical Simulation of Multiple Cracking in ANSI 304 Stainless Steel Under Thermal Fatigue, Int. J. Damage Mech, 19(7) (2010) 767-785.

[3] H.M. Westergaard, Bearing pressures and cracks, J. Appl. Mech, 6(2) 1939 49-53.

[4] N.I. Muskhelishvili, J. Radok, Some basic problems of the mathematical theory of elasticity, Cambridge Univ Press, 1953.

[5] O.L. Bowie, Analysis of an infinite plate containing radial cracks originating at the boundary of an internal circular hole, J. Math. Phys, 35(1) (1956) 60-71.

[6] P.B. Wang, Z.H. Yao, T. Lei, Analysis of solids with numerous microcracks using the fast multipole DBEM, Cmc-Comput Mater Con, 3(2) (2006) 65-75.

[7] P.B. Wang, Z.H. Yao, H.T Wang, Fast multipole BEM for simulation of 2-D solids containing large numbers of cracks, Tsinghua Sci \& Technol, 10(1) (2005) 76-81.

[8] Q.H. Qin, Y.W. Mai, BEM for crack-hole problems in thermopiezoelectric materials, Eng. Fract. Mech, 69(5) (2002) 577-588.

[9] E.D. Leonel, W.S. Venturini, Dual boundary element formulation applied to analysis of multi-fractured domains, Eng Anal Bound Elem, 34(12) (2010) 1092-1099.

[10] X. Q. Yan, A boundary element analysis for stress intensity factors of multiple circular arc cracks in a plane elasticity plate, Appl. Math. Model, 34(10) (2010) 2722-2737.

[11] Q. Xu, H.C. Sun, Virtual boundary element least square method for solving three dimensional problems of thick shell. J Dalian Univ Technol 36 (1996) 413-418. in Chinese.

[12] Q. Xu, H.C. Sun, Virtual boundary element least-square collocation method, Chin J Comput Mech,14 (1997) 166-73. in Chinese.

[13] H.C Sun, L.Z Zhang, Q. Xu, Y.M Zhang, Nonsingularity boundary element methods, Dalian: Dalian Univ. Techno. Press, (1999). in Chinese.

[14] Q. Xu, Three-Dimension virtual Boundary element method for solving the problems of thin shells, Chin J Appl Mech, 17 (2000) 111-115. in Chinese.

[15] Q. Xu, H.C Sun, Unified way for dealing with three-dimensional problems of solid elasticity, Appl Math Mech, 22 (2001) 1357-1367.

[16] Q. Xu, Z.J. Zhang, W. Si, Virtual boundary meshless least square collocation method for calculation of 2D multi-domain elastic problems, Eng Anal Bound Elem, 36(5) (2012) 696-708.

[17] D.S. Yang, Q. Xu, Virtual boundary meshless least square integral method with moving least squares approximation for 2D elastic problem, Eng Anal Bound Elem, 37(3) (2013) 616-623.

[18] Q. Xu, A new high-precision boundary-type meshless method for calculation of multidomain steady-state heat conduction problems, Numerical Heat Transfer, Part B, 64 (2013) 388-406.

[19] Q. Xu, D.S. Yang, Solving multi-domain 2D heat conduction problems by the least squares collocation method with RBF interpolation on virtual boundary, Eng Anal Bound Elem, 42 (2014) 37-44.

[20] G. R. Liu, Y. T. Gu, Boundary meshfree methods based on the boundary point interpolation methods, Eng Anal Bound Elem, 28(5) (2004) 475-487.

[21] Gu Y.T., Liu G.R., A boundary point interpolation method for stress analysis of solids, Computational Mechanics. 28, 2002, pp. 47-54.

[22] Gu, Y.T., Liu G.R., A boundary radial point interpolation method (BRPIM) for 2D meshless structure analysis, Structural engineering and mechanics, vol. 15, pp. 535-550, 2003.

[23] Liu G.R., A Point Assembly Method for Stress Analysis for Solid, in Impact Response of Materials & Structures, V. P. W. Shim et al. eds, Oxford, pp. 475-480, 1999.

[24] Wang J.G., Liu G.R., Radial point interpolation method for elastoplastic problems. Proc. of the 1st Int. Conf. On Structural Stability and Dynamics, Dec. 7-9, 2000, Taipei, Taiwan, pp. 703-708, 2000.

[25] Liu G.R., Mesh Free Methods: Moving Beyond the Finite Element Method. CRC press, Boca Raton, USA, 2002.
[26] Gu Y.T., Liu G.R., Using radial function basis in a boundary-type meshless method, boundary point interpolation method (BPIM), Inter. Conf. On Sci. & Engr. Comput., March 19-23, 2001a, Beijing. 68.
[27] Gu Y.T., Liu G.R., A boundary point interpolation method (BPIM) using radial function basis, First MIT Conference on Computational Fluid and Solid Mechanics, June 2001b, MIT, pp. 1590-1592.
[28] Wu Z.M., Compactly supported positive definite radial function, Advance in computational mathematics, vol. 4, pp. 283-292, 1995.
[29] China Aviation Research Institute, Handbook of stress intensity factor, Beijing: Science Press, 1993: 3, 68,134. in Chinese.
[30] LI Zailiang, WANG Cheng. Higher Boundary Element Method, Beijing: Science Press, 2008: 262-263. in Chinese.
[31] Tuhkuri J. Dual boundary element analysis of closed cracks[J]. International Journal for Numerical Methods in Engineering, 1997, 40(16): 2995-3014.
[32] Yan X., Interaction of arbitrary multiple cracks in an infinite plate, The Journal of Strain Analysis for Engineering Design, 2004, 39(3): 237-244.
[33] Chen Y Z., Stress intensity factors for curved and kinked cracks in plane extension, Theoretical and Applied Fracture Mechanics, 1999, 31(3): 223-232.